Dalton Transactions

ROYAL SOCIETY OF CHEMISTRY

PAPER

View Article Online
View Journal

Cite this: DOI: 10.1039/d4dt01740d

Ru(II)–arene azole complexes as anti-amyloid-β agents†

Ryan M. Hacker,[a] Daniela M. Grimard,[a] Katie A. Morgan,[a] Eaman Saleh,[b] Morgan M. Wrublik,[b] Cade J. Meiss,[b] Caitlyn C. Kant,[b] Marjorie A. Jones,[b] William W. Brennessel[c] and Michael I. Webb*[a]

Received 14th June 2024,
Accepted 26th July 2024

DOI: 10.1039/d4dt01740d

rsc.li/dalton

With the recent clinical success of anti-amyloid-β (Aβ) monoclonal antibodies, there is a renewed interest in agents which target the Aβ peptide of Alzheimer's disease (AD). Metal complexes are particularly well-suited for this development, given their structural versatility and ability to form stabile interactions with soluble Aβ. In this report, a small series of ruthenium–arene complexes were evaluated for their respective ability to modulate both the aggregation and cytotoxicity of Aβ. First, the stability of the complexes was evaluated in a variety of aqueous media where the complexes demonstrated exceptional stability. Next, the ability to coordinate and modulate the Aβ peptide was evaluated using several spectroscopic methods, including thioflavin T (ThT) fluorescence, dynamic light scattering (DLS), and transmission electron microscopy (TEM). Overall, the complex **RuBO** consistently gave the greatest inhibitory action towards Aβ aggregation, which correlated with its ability to coordinate to Aβ in solution. Furthermore, **RuBO** also had the lowest affinity for serum albumin, which is a key consideration for a neurotherapeutic, as this protein does not cross the blood brain barrier. Lastly, **RuBO** also displayed promising neuroprotective properties, as it had the greatest inhibition of Aβ-inducted cytotoxicity.

Introduction

First described by Dr Alois Alzheimer over 100 years ago,[1] the disease that now bears his name has unfortunately become a significant burden to the health care system. Currently, an estimated 6.9 million Americans over the age of 65 are living with Alzheimer's disease (AD), while the costs associated with treatments are estimated at $360 billion.[2] Two of the cardinal pathological hallmarks of AD are extracellular senile plaques and interfibrillar tangles. The latter of which are due to hyperphosphorylation of the protein tau, while the former are comprised primarily of the small peptide amyloid-beta (Aβ).[3] Aβ is a 40–42 amino acid long peptide that is synthesized following the enzymatic cleavage of the transmembrane amyloid-precursor protein. Depending on the location of the secretase enzyme excision, either $Aβ_{40–42}$ or the p3 peptide is made.[4]

The observation of high concentrations of Aβ within the senile plaques of AD patent brains led to the proposed "amyloid cascade hypothesis" in 1992,[5] and significant interest in the development of therapeutic approaches to target this species.[6] Such efforts have been rewarded by the recent FDA approval of two monoclonal antibodies which target the soluble form of Aβ, resulting in diminished plaque formation and forestalling of the progression of the disease.[7] While such therapeutics are laudable, the elevated costs associated with such treatments necessitates the development of cheaper, yet equally effective, alternatives.

Within Aβ plaques of AD brains there are elevated concentration of metal ions relative to the nearby surrounding tissues, which suggests there is a link between dysregulation of metal ion homeostasis and AD progression.[8] Metal-based complexes can exploit this affinity of Aβ for free metal ions by forming stable interactions with the peptide, such that its aggregation in minimized.[9] The first metal-based complexes to specifically target the Aβ peptide were cationic ^{99m}Tc compounds such as (**1**) in Fig. 1, which contained bipyridyl-linked aromatic azo dye ligands. These complexes were used to detect $Aβ_{40}$ and had similar affinity relative to established organic dyes.[10] This spurred the development of subsequent metallotherapeutics which could target, and prevent and aggregation of the Aβ peptide. Beginning with the platinum(II) complex (**2**) which was observed to substantially limit the aggregation and cytotoxicity of $Aβ_{42}$.[11] This was achieved *via* coordinate interactions with the histidine residues of the

[a]*Department of Chemistry and Biochemistry, SUNY Geneseo, Geneseo, NY, 14454, USA. E-mail: mwebb@geneseo.edu*
[b]*Department of Chemistry, Illinois State University, Normal, IL, 61790, USA*
[c]*Department of Chemistry, University of Rochester, Rochester, NY, 14627, USA*

†Electronic supplementary information (ESI) available. CCDC 2356322–2356324. For ESI and crystallographic data in CIF or other electronic format see DOI: https://doi.org/10.1039/d4dt01740d

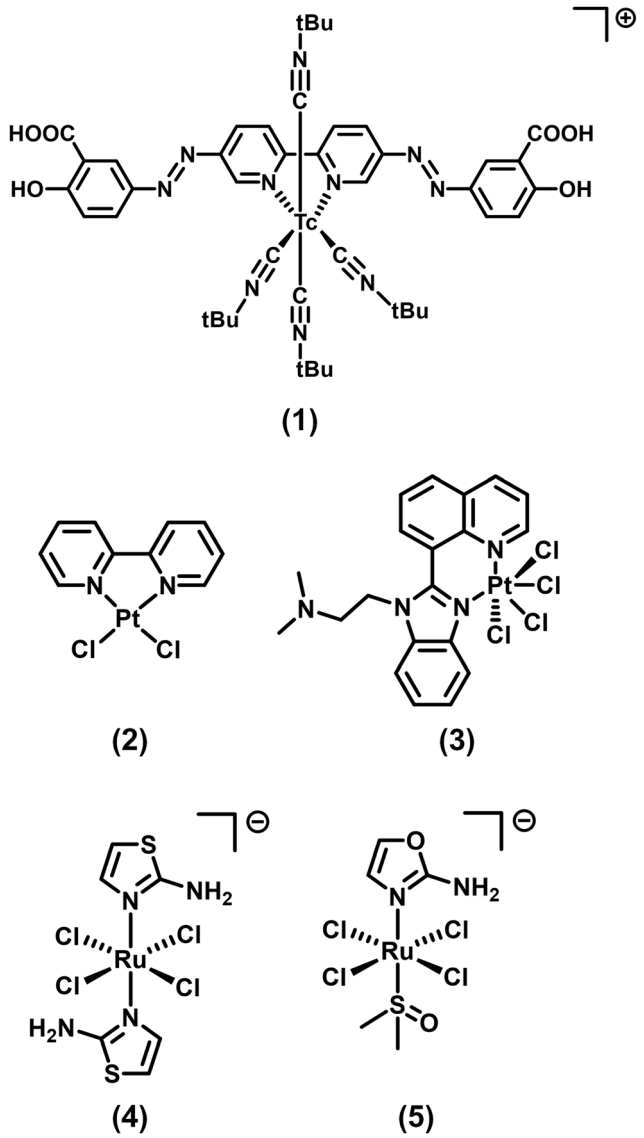

Fig. 1 Metal-based complexes evaluated for their ability to target and/or modulate the aggregation and cytotoxicity of the Aβ peptide.

peptide, while the 1,10-phenanthroline ligand afforded additional hydrophobic interactions.[12] This led to the development of the orally-available Pt(IV) complex (**3**) which was able to decrease the occurrence of Aβ plaques within brain of APP/PS1 mice.[13]

To date, complexes of 27 different metals have been evaluated, with varying success, for their ability to target the Aβ peptide.[14] Of these, ruthenium complexes have shown substantial promise, particularly with regards to detailed structure–activity relationships (SAR), where in comparing the activity of (**4**) and (**5**), symmetry around the Ru metal center did not significantly impact the activity of the complexes, rather, the inclusion of a primary amine on the heterocyclic ligand in resulted in the greatest anti-Aβ activity.[15–17] This is likely due to hydrogen bonding interactions with the Aβ peptide, which provide a multi-modal coordination mode, similar to that observed for (**2**). Additionally, varying the heteroatom within the azole ring was also found to impact the performance of the complexes, where the oxazole containing complexes had greater anti-Aβ activity relative to their imidazole and thiazole analogs.

To further these SAR studies, five Ru(II)–arene complexes were prepared and evaluated for their ability to modulate the aggregation and cytotoxicity of Aβ (Fig. 2). The inclusion of the 2-aminoazole ligand leverages the established SAR for Ru complexes, while offering a new avenue for development. Despite being well-established in the field of cancer therapeutics,[18–20] Ru–arene complexes have seen limited investigation in AD therapy,[21–23] with the current study providing vertical growth in the quest for novel anti-Aβ AD therapeutics.

Experimental

Materials and methods

All reagents and materials were used as received from the manufacturer, unless otherwise noted. The chemicals used in the synthesis and biological assays were purchased from Ambeed (1*H*-benzo[*d*]imidazol-2-amine, benzo[*d*]oxazol-2-amine, benzo[*d*]thiazol-2-amine), Oakwood Chemical (1,1,1,3,3,3,-hexafluoro-2-propanol (HFIP), 2-aminothiazole, oxazol-2-ylamine), Sigma-Aldrich (ruthenium(III) chloride hydrate), TCI America (dansyl glycine), and Thermo Fisher (alpha-terpinene, chloroform, deuterium oxide, dimethyl sulfoxide, methanol, methyl sulfoxide-D_6, hexanes). Human serum albumin (HSA) was obtained as a lyophilized powder from Sigma Aldrich. $A\beta_{16}$ was purchased from 21st Century Biochemicals, $A\beta_{40}$ was purchased from APExBio, and $A\beta_{42}$ was purchased from GenScript. Both $A\beta_{40}$ and $A\beta_{42}$ were monomerized following established procedures prior to use.[24]

Elemental analysis (EA) data were collected at the Center for Enabling New Technologies Through Catalysis at the University of Rochester using a PerkinElmer 2400 Series II Analyzer.

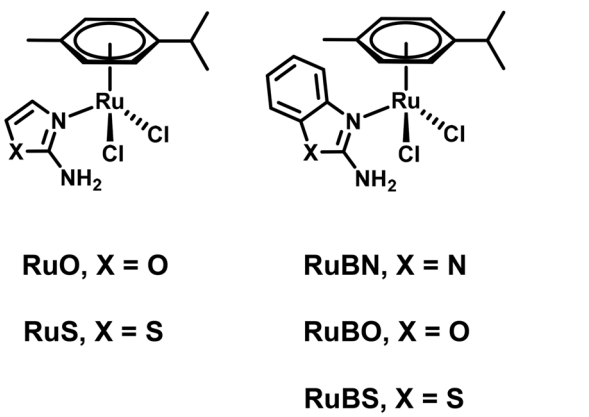

Fig. 2 The Ru–arene complexes prepared and evaluated herein for their anti-Aβ ability.

The ^{1}H and ^{13}C NMR in $CDCl_3$ or DMSO-D_6 were collected using either a Bruker Avance NEO 400 MHz NMR spectrometer or a Varian 400-MR 400 MHz NMR spectrometer. All D_2O/DMSO-D_6 ^{1}H NMR data were collected using the Varian spectrometer.

Diffraction data of single crystals were obtained using a Rigaku XtaLAB Synergy-S Dualflex diffractometer equipped with a HyPix-6000HE HPC area detector for data collection at 100 K. The full data collection was carried out using a PhotonJet (Cu) X-ray source. The structure was solved using SHELXT[25] and refined using SHELXL.[26] Most or all non-hydrogen atoms were assigned from the solution. Full-matrix least squares/difference Fourier cycles were performed which located any remaining non-hydrogen atoms. All non-hydrogen atoms were refined with anisotropic displacement parameters. The N–H hydrogen atoms were found from the difference Fourier map and refined freely. All other hydrogen atoms were placed in ideal positions and refined as riding atoms with relative isotropic displacement parameters. See ESI Tables S3–S5† for final refinement parameters.

Synthetic procedures

The Ru(II)–arene dimer ([Ru(η^6-*p*-cymene)Cl_2]$_2$) was prepared following a previous procedure.[27]

General synthesis of Ru–arene-azole complexes

The prepared Ru(II)–arene dimer (0.15 mmol) and azole ligand (0.30 mmol) were combined in methanol (6 mL) and heated to reflux for 2 hours. The resulting mixture was then stored at −20 °C overnight and solid precipitates were isolated the following day using vacuum filtration, then dried under high vacuum for several hours. Additional purification for each complex is noted, when applicable.

RuO (Ru(η^6-*p*-cymene)(2-aminooxazole)Cl_2). Red crystalline solid (0.0432 g, 32.3% yield). ^{1}H NMR (400 MHz, DMSO-D_6, ppm): 7.34 (1H, s), 6.68 (1H, s), 6.51 (2H, bs), 5.82 (2H, d), 5.78 (2H, d), 2.84 (1H, sept), 2.09 (3H, s), 1.19 (6H, d). ^{13}C NMR (100 MHz, DMSO-D_6): 18.29, 21.92, 30.39, 85.93, 86.78, 100.50, 106.78, 126.90, 126.92, 131.93, 161.92. EA results for $C_{13}H_{18}N_2OCl_2Ru$ theoretical: 40.00 C, 4.66 H, 7.18 N. Experimental: 40.00 C, 4.45 H, 7.07 N.

RuS (Ru(η^6-*p*-cymene)(2-aminothiazole)Cl_2). Red powder (0.1764 g, 66.4% yield). ^{1}H NMR (400 MHz, DMSO-D_6, ppm): 6.92 (1H, d), 6.84 (2H, bs), 6.54 (1H, d), 5.82 (2H, d), 5.78 (2H, d), 2.84 (1H, sept), 2.10 (3H, s), 1.20 (6H, d). ^{13}C NMR (100 MHz, DMSO-D_6): 18.28, 21.92, 30.39, 85.93, 86.78, 100.50, 106.78, 106.91, 139.03, 169.21. EA results for $C_{13}H_{18}N_2SCl_2Ru$ theoretical: 38.42 C, 4.47 H, 6.90 N. Experimental: 38.27 C, 4.24 H, 6.74 N.

RuBN (Ru(η^6-*p*-cymene)(2-aminobenzimidazole)Cl_2). Additional recrystallization used 1 : 2 chloroform : hexanes yielding the product as a mustard yellow powder (0.1170 g, 40.8% yield). ^{1}H NMR (400 MHz, $CDCl_3$, ppm): 9.06 (1H, s), 7.47 (1H, d), 6.79 (1H, t), 6.49 (1H, t), 6.18 (1H, s), 6.03 (2H, s), 5.50 (2H, s), 5.21 (2H, s), 2.93 (1H, sept), 1.81 (3H, s), 1.22 (6H, d). ^{13}C NMR (100 MHz, DMSO-D_6): 18.29, 21.92, 30.39, 30.62, 85.93, 86.78, 100.51, 106.79, 119.45, 155.50. EA results for $C_{17}H_{21}N_3Cl_2Ru$ theoretical: 46.47 C, 4.83 H, 9.57 N. Experimental: 46.30 C, 4.68 H, 9.35 N.

RuBO (Ru(η^6-*p*-cymene)(2-aminobenzoxazole)Cl_2). Tangerine-colored powder (0.1011 g, 67.3% yield). ^{1}H NMR (400 MHz, DMSO-D_6, ppm): 7.30 (2H, bs), 7.25 (1H, dd), 7.14 (1H, dd), 7.03 (1H, td), 6.90 (1H, td), 5.78 (2H, d), 5.73 (2H, d), 2.78 (1H, sept), 2.04 (3H, s), 1.14 (6H, d). ^{13}C NMR (100 MHz, DMSO-D_6): 18.29, 21.92, 30.39, 85.93, 86.78, 100.50, 106.78, 108.81, 115.67, 120.34, 123.87, 144.02, 148.33, 163.12. EA results for $C_{17}H_{20}N_2OCl_2Ru$ theoretical: 46.36 C, 4.59 H, 6.36 N. Experimental: 46.28 C, 4.53 H, 6.09 N.

RuBS (Ru(η^6-*p*-cymene)(2-aminobenzothiazole)Cl_2). Additional recrystallization used 1 : 1 chloroform : hexanes yielding the product as a dark orange powder (0.0591 g, 19.8% yield). ^{1}H NMR (400 MHz, DMSO-D_6, ppm): 7.59 (1H, dd), 7.42 (2H, s), 7.28 (1H, dd), 7.15 (1H, td), 6.95 (1H, td), 5.77 (2H, d), 5.73 (2H, d), 2.78 (1H, sept), 2.04 (3H, s), 1.14 (6H, d). ^{13}C NMR (100 MHz, DMSO-D_6): 18.29, 21.92, 30.39, 85.93, 86.78, 100.50, 106.78, 118.09, 121.24, 121.30, 125.85, 129.32, 131.24, 166.84. EA results for $C_{17}H_{20}N_2SCl_2Ru$ theoretical: 44.73 C, 4.43 H, 6.14 N. Experimental: 45.03 C, 4.46 H, 5.91 N.

Log *D*

Stock solutions of each Ru complex were prepared by dissolution in dimethyl sulfoxide (DMSO) then dilution to 50 μM using phosphate buffered saline (PBS, pH 7.4) with a final DMSO concentration of ≤1%. Each sample was prepared in triplicate. The absorbance spectra for the aqueous samples were measured, then an equal volume of 1-octanol was added and the resulting biphasic samples were mixed for 2 hours at room temperature using an IKA Trayster inversion mixer (60 rpm). Following this, the aqueous layers were extracted and their absorbance spectra were measured. The resulting log *D* values were calculated using the equation below:

$$D = \log\left(\frac{\text{Abs@}\lambda_{\max}\text{ before mixing}}{\text{Abs@}\lambda_{\max}\text{ after mixing}}\right) - 1.$$

UV-Vis sample preparation and analysis

Each Ru complex was initially dissolved in DMSO then diluted using PBS to achieve a final concentration of 100 μM, where the DMSO content was 5% or less. UV-Vis spectra were measured using a Cary 50 Spectrophotometer equipped with a single cell Peltier system where the sample temperature was maintained at either 25 °C or 37 °C. The absorbance of each sample was measured from 220 nm–800 nm, with data collection occurring every minute for the first 30 minutes, followed by every 10 minutes for up to 6 hours.

For the samples which contained $A\beta_{16}$, stock solutions of the peptide were prepared in pure DMSO, followed by the addition of a stock solution of the Ru complex. Dilution using PBS afforded an equimolar amount of $A\beta_{16}$ and Ru (100 μM) and a DMSO concentration that was ≤5%. Spectra were measured at 37 °C using the same instrumentation and parameters as above.

Imidazole binding

Samples of the Ru complexes were mixed with equimolar amount of histidine and the resulting mixtures were measured using ^{1}H NMR and UV-Vis spectroscopy. For the ^{1}H NMR study, both the Ru complex and imidazole were dissolved in $CDCl_3$ and the spectrum was measured immediately following dissolution. For the UV-Vis study, the Ru complex and imidazole were initially dissolved in DMSO then diluted using PBS to achieve a final concentration of 100 μM of both molecules, where the DMSO content was 5% or less. UV-Vis spectra were then measured as described above, where the sample temperature was maintained at 37 °C.

Thioflavin T fluorescence assay

The aggregation assay was performed following previously reported procedures,[15,28] where thioflavin T (ThT) fluorescence was measured with a Varioskan LUX plate reader using λ_{ex} = 450 nm and λ_{em} = 485 nm. Statistical analysis was performed using a one-way analysis of variance (ANOVA).

DLS sample preparation

The DLS samples were taken directly from the ThT assay where a 60 μL aliquot from a sample well was filtered using a 0.2 μm syringe filter. A 20 μL aliquot from this filtrate was subsequently placed in a folded capillary cell (DTS1070). Measurements were then made using a Malvern Zetasizer Nano ZSP, where the cumulant data (percent intensity) is represented as an average measurement consisting of sub-runs determined by the Zetasizer software Version 7.13.

TEM sample preparation

Samples for TEM imaging were obtained from the remaining DLS filtrates, where a 10 μL aliquot was added to a 300-mesh formvar-coated copper grid and allowed to stabilize for 2 minutes. The solvent was then wicked away, and the samples were then stained using 10 μL of 2% uranyl acetate, which coated the sample for 60 seconds before being wicked away. Excess salts were washed away as 10 μL of H_2O was added to the grids, left for 30 seconds, then wicked away. The prepared grids were stored at room temperature until analysis. All imaging measurements were made at the High Resolution Transmission Electron Microscopy (HRTEM) facility at the University at Buffalo using a JEOL JEM 2010 High Resolution Transmission Electron Microscope operating at 200 kV and 20 000× magnification.

HSA binding assay

Fluorescence competition experiments were performed following previously reported procedures.[29] A stock solution of HSA (100 μM) was prepared using only PBS, while stock solutions of dansyl glycine (DG, 50 μM) and each Ru complex (50 μM) were prepared by initial dissolution in DMSO followed by immediate dilution using PBS to give a DMSO concentration of ≤1%. Individual samples were prepared by first mixing HSA and DG, followed by the addition of the respective Ru complex. The total volume of each sample was 3 mL where the concentrations of HSA and DG remained constant (2.5 μM) and the Ru concentration ranged from 0 μM to 25 μM. The samples were then placed in a 28 °C water bath for 15 minutes before the fluorescence spectra were measured. Fluorescence measurements were recorded at room temperature using a PTI QuantaMaster 50. The excitation wavelength was set to 335 nm and the emission spectra were collected from 350 nm to 600 nm.

Cytotoxicity screening

Evaluation of the Ru complexes to prevent $A\beta_{42}$-induced cytotoxicity towards axenic *Rattus norvegicus* C6 glioma cells (ATCC CCL-107) followed previously reported procedures.[16] The respective Ru complexes (20 μM) and $A\beta_{42}$ (20 μM) were added to cultured cells and incubated for 24 hours at 37 °C in a 5% CO_2 environment. Cell viability was determined using a 3-(4,5-dimethylthiazol-2-yl)-2,5-diphenyltetrazolium bromide (MTT) assay performed in quadruplicate with the results reported as the mean ± the standard deviation.

Results and discussion

Synthesis and characterization

The Ru–arene complexes were all prepared in a similar manner from a Ru(II)–arene dimer. The resultant complexes were isolated in reasonable yields, and initially characterized using ^{1}H and ^{13}C NMR (ESI Fig. S1–S10†). For the novel complexes, **RuO**, **RuS**, and **RuBO**, crystals suitable for X-ray diffraction were isolated and their structures were solved (Fig. 3). All three complexes exhibit the anticipated "piano-stool" type geometry which is typical for such Ru–arene complexes containing an η^6-aromatic ligand.[20] The respective azole ligands are coordinated to the Ru metal center *via* the imine nitrogen, while two chloride ligands complete the octahedral coordination sphere. Upon analysis, the Ru–N azole bond length was 2.125(19) Å for **RuO**, 2.136(4) Å for **RuS**, and 2.134(15) Å for **RuBO**. These values are in good agreement with those of **RuBN** (2.133(8) Å) and **RuBS** (2.169(18) Å).[30]

Ligand exchange and partitioning

Metal-based therapeutics are often classified as prodrugs, whereby the synthesized complex(es) are activated within cellular environments, such as *via* aqueous ligand exchange, which then facilitates coordination to their biological target, eliciting their biological activity.[31] To determine the relative stability and rate of such exchange, the prepared complexes were evaluated using the two complementary spectroscopic methods of NMR and UV-Vis. Beginning with the UV-Vis study, all of the complexes were initially dissolved in DMSO prior to dilution using PBS to achieve a final concentration of 100 μM with ≤5% DMSO. Spectra for the samples were then measured following extended incubation. Somewhat surprisingly, no significant changes were observed when comparing the initial spectrum to the final spectrum, measured after 6 hours

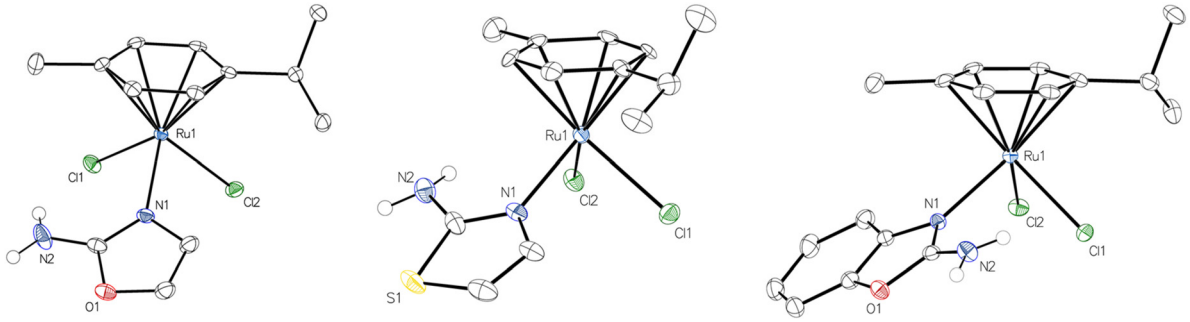

Fig. 3 X-ray crystal structures of complexes **RuO**, **RuS**, and **RuBO** where any co-crystallizing solvent molecules have been omitted for the sake of clarity. The ellipsoids of all non-hydrogen atoms are shown at the 50% probability level.

(Fig. 4A and ESI Fig. S11–S15†). This suggests that our complexes are reasonably stable in buffered aqueous media, mirroring results that have been observed for other Ru(II)–arene complexes.[32,33] Interestingly, this is in stark contrast to the Ru(II)–arene anticancer complex RAPTA-C, where significant changes were observed within 15 minutes of incubation under physiological conditions.[34] The lone difference between our prepared Ru complexes and RAPTA-C are the 2-aminoazole ligands which replace the PTA (1,3,5-triaza-7-phosphatricyclo-[3.3.1.1]-decane) ligand, suggesting that the new ligands may improve the stability of our complexes.

To probe the impact of the chloride ions on the ligand exchange, the UV-Vis spectra of the Ru complexes were measured in unbuffered water. Even in the absence of buffering agents, the spectra were virtually identical following prolonged mixing (ESI Fig. S16–S20†). To confirm their aqueous stability, the Ru complexes were subjected to ^{1}H NMR analysis following dissolution in D_2O with 10% DMSO-D_6. These samples were then subjected to similar incubation times to the UV-Vis samples, allowing for a qualitative comparison of the relative rate and extent of ligand exchange. Even in the absence of incubation, substantial changes in the ^{1}H NMR spectra were observed for all 5 complexes, as new peaks emerged in close proximity to those of the parent complex, such as those shown in Fig. 4B for **RuBO** in the aromatic region of the spectrum. Interestingly, despite the rapid occurrence of the peaks, their intensities did not change upon extended incubation, suggesting that the ligand exchange that occurred was complete and rapid. This highlights the importance of multiple spectroscopic methods for analysis, as such exchange was not visible within the absorbance spectra. Similar phenomena has been observed for other Ru(II)–arene complexes following dissolution in unbuffered aqueous media, highlighting the impact of the chloride ions on forestalling exchange.[23,35]

An important aspect in the mechanism of action of a potential therapeutic is its ability to partition between aqueous and organic media, as this serves as a marker for potential diffusion across cell membranes.[36] Such partitioning is commonly referred to as $\log P$, which uses pure water and 1-octanol, a long chain alcohol which mimics a fatty acid, to determine the relative hydrophilic/hydrophobic partitioning. However, given the aforementioned instability of the complexes in pure water, the partitioning of the complexes was evaluated using a mixture of PBS and 1-octanol. This yields a $\log D_{7.4}$ value, which provides a physiological representation of the partitioning. Using the shake-flask method,[37] equal volumes of 1-octanol and PBS were combined where the relative amount of the complexes present within the aqueous layer was monitored before and after mixing. Only **RuO** preferred the aqueous layer, while all the remaining complexes partitioned to the organic fraction. This correlates with the increased hydrophobicity of the 2-aminobenzoazole ligands, whereby **RuBS** had the largest $\log D_{7.4}$, followed by **RuBN**, and **RuBO** (Table 1). In order for a potential neurotherapeutic to passively diffuse across the blood–brain barrier (BBB), a $\log D$ in the range of 1–4 has been observed to be optimal.[38] While the prepared compounds fall just outside of this range, they do adhere to other central nervous system (CNS) drug metrics such as number of hydrogen bond donors ($\leq$3) and acceptors ($\leq$7).[39]

To provide an important comparison to our experimentally determined $\log D_{7.4}$ values, the relative lipophilicity of the complexes was calculated using the open-source software SWISS ADME.[40] Since all of the complexes are neutral, this facilitated the modeling of the complexes using the software, and the simplified molecular-input line-entry system (SMILES) for each molecule is included in the ESI (Table S1).† Comparing the partitioning values yielded the same trend for increasing lipophilicity with **RuO** being the lowest and **RuBS** having the highest $\log P$. However, the calculated values were substantially higher than the experimentally determined ones, necessitating such experiments for metal-based complexes.

Aβ binding

Metal complexes which target Aβ are thought to coordinate to the histidine residues (His-6, His-13, and His-14) within the peptide.[41,42] Such coordination forestalls the natural self-association of Aβ, thereby resulting in decreased aggregation of the peptide.[12] To determine the ability of the prepared complexes to coordinate to Aβ, a truncated version of the peptide was used ($A\beta_{16}$). This variant contains the three histidine residues of interest, while having no propensity to aggregate in

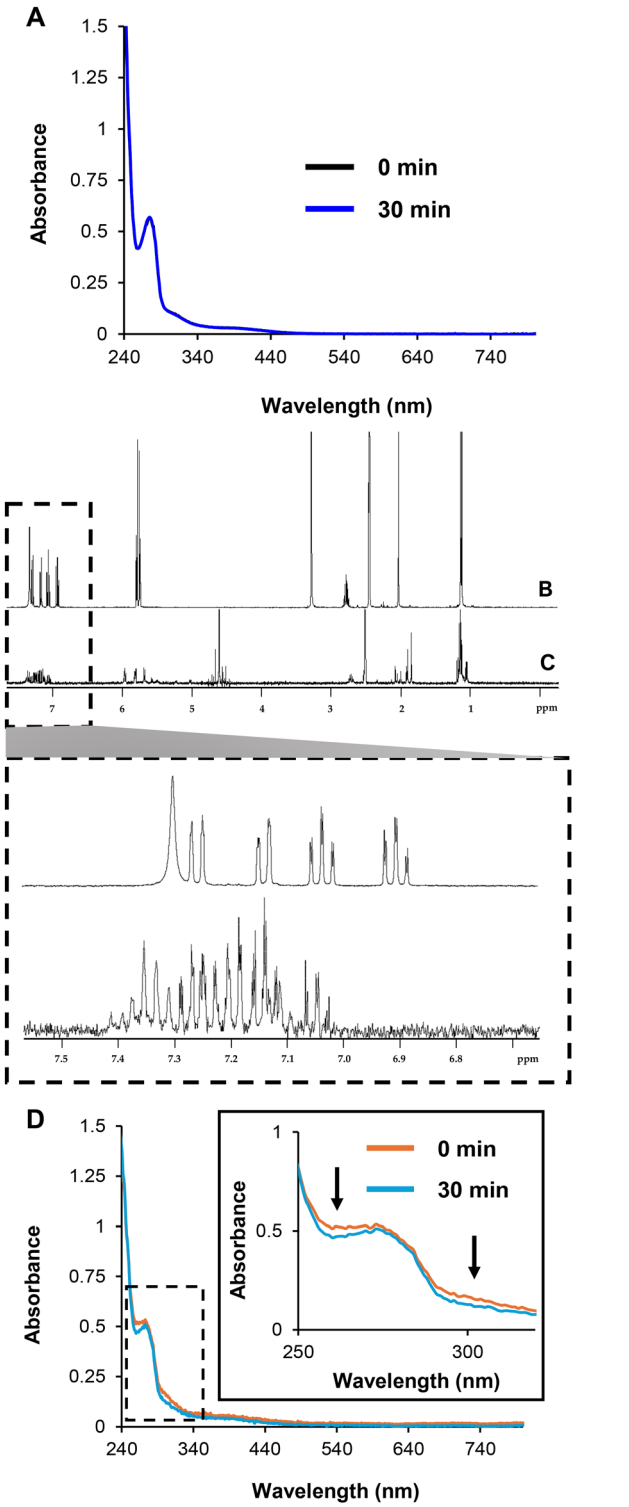

Fig. 4 Aqueous stability and $A\beta_{16}$ binding data for **RuBO**. (A) UV-Vis spectra of 100 μM **RuBO** in PBS with incubation at 37 °C for 30 minutes, (B) ^{1}H NMR of **RuBO** in DMSO-D_6, (C) ^{1}H NMR **RuBO** in D_2O and 10% DMSO-D_6 with no incubation (inset: the aromatic region of the spectra), (D) UV-Vis spectra of 100 μM **RuBO** in PBS with 100 μM $A\beta_{16}$ with incubation at 37 °C for 30 minutes.

Table 1 The experimentally determined log $D_{7.4}$ values for each Ru complex juxtaposed with the calculated log P values, along with the conditional binding constants to serum albumin

Complex	Log $D_{7.4}$	Calculated log P	Log K'
RuO	−0.601 ± 0.180	2.09	4.21
RuS	0.022 ± 0.139	2.65	4.48
RuBN	0.408 ± 0.037	3.11	4.33
RuBO	0.380 ± 0.093	3.07	3.89
RuBS	0.873 ± 0.140	3.63	3.96

solution.[43] Samples containing equimolar amounts of $A\beta_{16}$ and each Ru complex were analyzed using UV-Vis spectroscopy. Such analyses would provide a direct comparison to the free complexes in solution, whereby any changes to the spectra would be indicative of peptide binding. For several of the complexes minor changes to the spectra were observed within the first 30 minutes of incubation. A consistent decrease in the signals around 270 nm occurred for **RuO** (Fig. S26†), **RuS** (Fig. S27†), and **RuBO** (Fig. 4D and S29†), while no such change was observed for **RuBN** (Fig. S28†) and **RuBS** (Fig. S30†). With extended incubation for up to 6 hours only **RuO** exhibited a continued decrease in the same peak, while all the other Ru complexes remained virtually unchanged. Although only minor changes were observed in the spectra for 3 complexes, these are substantially different from all previously described spectra in aqueous media alone where no changes were observed. Given this disparity, such changes are attributed to a coordinate interaction between the Aβ peptide and the Ru complexes, specifically **RuO**, **RuS**, and **RuBO**. However, similar to the previous discussion on ligand exchange, the absence of change in the spectra does not preclude the occurrence of peptide binding for **RuBN** or **RuBS**, such associations are unfortunately not observed using this method.

To evaluate the potential coordination of the complexes to Aβ *via* histidine, an additional study was performed where each complex was mixed with an equimolar amount of imidazole. For these studies, samples were measured using the complementary methods of ^{1}H NMR and UV-Vis. Beginning with ^{1}H NMR, samples were initially prepared similar to those of the stability assay, using 10% D_6-DMSO in D_2O. Unfortunately, this resulted in similar spectra to the original stability samples, where numerous signals emerged in the aromatic region of the spectra, therefore the aqueous media was replaced with organic solvents. Following immediate dissolution and mixing the resulting ^{1}H NMR spectrum for each complex in the presence of imidazole was substantially changed (Fig. S31–35†). In each case, signals from the free imidazole were noticeably absent, while new signals emerged, suggesting that coordination of the imidazole to the Ru metal center occurred. This was further supported by the UV-Vis spectra of the complexes following extended incubation with imidazole (Fig. S36–40†). Indeed, changes in the spectra were observed for only **RuO**, **RuS**, and **RuBO**, where a similar phenomenon to the spectra following mixing with $A\beta_{16}$

occurred, with a discernable decrease in signals observed around 300 nm. By contrast, the spectra for **RuBN** and **RuBS** remained constant, which again mirrors the observations from those complexes with $A\beta_{16}$. Taken together, these results support the likelihood of coordination of $A\beta_{16}$ to the Ru metal center *via* histidine imidazole.

ThT fluorescence

A common method of evaluating the anti-amyloid ability of potential AD therapeutics is determining their impact on the aggregation of the full-length Aβ peptide. This can be monitored using a variety of methods, arguably the most common of which is fluorescence using a spectrochemical probe, such as thioflavin T (ThT).[44] In the presence of Aβ aggregate species, ThT emits a characteristic fluorescence peak around 485 nm, which is caused by a loss of the free rotation about the benzothiazole.[45] This has been shown to be a quantifiable metric for the extent of Aβ aggregation,[46] allowing for the facile comparison between potential AD therapeutics and their respective anti-Aβ ability.

For the evaluation of the complexes, the concentration of each Ru complex was consistent (10 μM) and equimolar to the $A\beta_{40}$ peptide. The complexes were all incubated with the peptide for 24 hours, after which the fluorescence measurements were taken. The $A\beta_{40}$ peptide in the absence of any Ru complexes was used as the positive control and scaled to be the maximum extent of aggregation. Overall, it was found that all complexes caused a statistically significant decrease in the observed aggregation of the peptide (Fig. 5). The least active complex was **RuBS** (30 ± 13%), followed by **RuBN** (20 ± 16%). The greatest inhibitory activity was observed for **RuBO** (8.9 ± 7.1%), followed closely by **RuO** (10 ± 2.2%), and **RuS** (10 ± 6.0%). Both **RuO** and **RuS** show a substantial improvement over previous Ru(III) which used the same amino-azole ligand,[15,16] while the activity of **RuBO** is among the greatest measured for a Ru(II)–arene complex to date. These initial results suggest that association with the Aβ peptide, as discussed previously by UV-Vis, likely impacted the resultant performance of the complexes. This is corroborated by the observation that **RuBN** and **RuBS**, for which no changes in the $A\beta_{16}$ UV-Vis spectra were observed, had substantially less activity in comparison to their counterparts. Furthermore, the two complexes that gave the greatest inhibitory activity, **RuBO** and **RuO**, have an oxazole ring, a feature that has been suggested to impart hydrogen-bonding with the peptide,[16] thereby having a greater impact on modulation its aggregation.

DLS

Aggregation of the Aβ peptide commonly results in deposits of variable size,[47] which are ideal for analysis using DLS, as this technique is sensitive to large particle sizes in solution, providing size distribution profiles of the species detected.[48] We have successfully used this technique in the previous evaluation of Ru complexes that modulate the aggregation of Aβ.[15,16,28,49] For the current study, the samples used for DLS were taken directly from the ThT assay, and filtered prior to analysis. In the absence of any Ru complex, the Aβ peptide gave a broad signal with an average particle size of 233.4 nm. Following incubation with the respective Ru complexes, a discernable shift to smaller particle sizes was observed with a concomitant

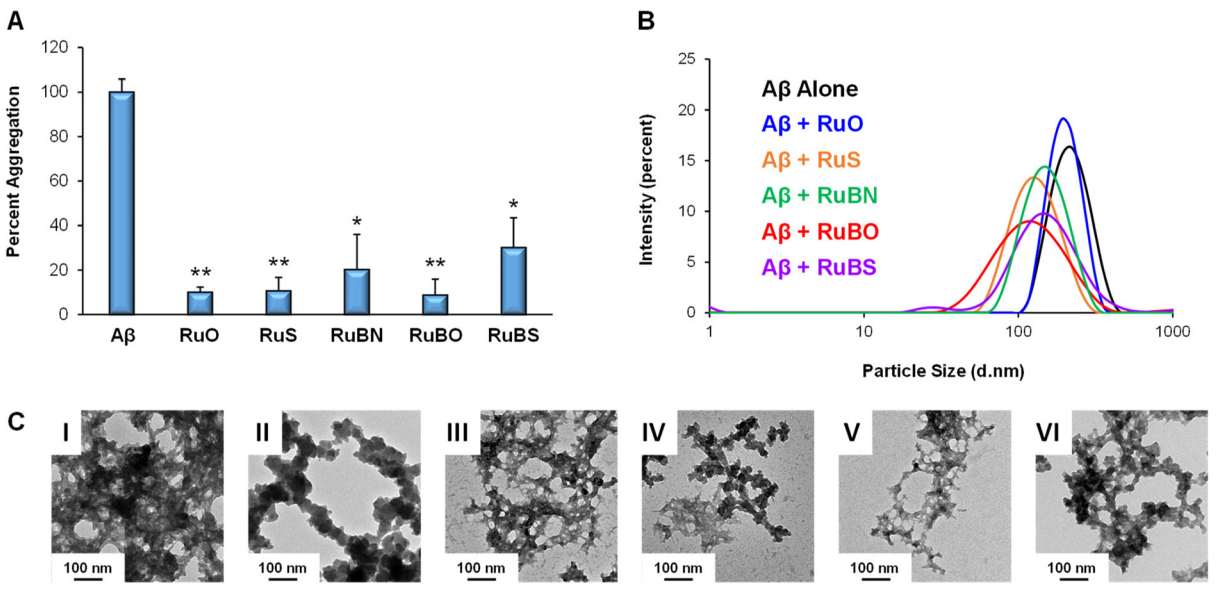

Fig. 5 Aβ aggregation assay results, following the incubation of equimolar solutions (10 μM) of $A\beta_{40}$ with the Ru complexes for 24 h at 37 °C. (A) ThT fluorescence results, where the signals were normalized to the positive control of the free peptide in solution. *P < 0.05 and **P < 0.001 for the treatments relative to $A\beta_{40}$ alone following statistical analysis by a one-way ANOVA. (B) DLS spectra obtained from filtrates of the ThT samples. (C) TEM images taken at 20 kX magnification of the DLS filtrates: (I) $A\beta_{40}$ alone, (II) $A\beta_{40}$ + **RuO**, (III) $A\beta_{40}$ + **RuS**, (IV) $A\beta_{40}$ + **RuBN**, (V) $A\beta_{40}$ + **RuBO**, (VI) $A\beta_{40}$ + **RuBS**.

broadening of the signal, providing greater intensity at smaller particle sizes, relative to the peptide alone. The largest particle sizes were observed following incubation with **RuO** (204.0 nm), followed by **RuBS** (168.0 nm), **RuBN** (156.3 nm), **RuS** (135.0 nm), and **RuBO** (131.9 nm) as shown in Fig. 5B.

When compared to the ThT results, the only consistency was the performance of **RuBO**, which gave the smallest particle sizes. The low maximum intensity and broad distribution of the DLS signal for **RuBO** indicates that a substantial proportion of the species observed had small hydrodynamic radii. By contrast, the DLS signal for **RuO**, which had the second lowest percent aggregation from the ThT assay, was remarkably similar to that of Aβ, albeit slightly shifted to smaller sizes. The remaining three complexes had intermediate particle sizes, with **RuBS** having a bimodal signal, where a minor peak (~1.5% of the total signal) was observed at 30.4 nm. For most spectroscopic methods this would likely be within the noise; however, since DLS is a technique that is sensitive to larger particles,[50] the appearance of a peak signifies that such particles were indeed observed. This phenomenon has been observed previously,[17] and provides additional support for the modulation of Aβ aggregation by the complexes.

TEM imaging

The final method used in the evaluation of the Ru complexes to modulate the aggregation of $A\beta_{40}$ was visualizing the aggregate species using TEM. The samples used to prepare the TEM grids are identical to those from the ThT and DLS experiments, thereby providing a complete picture on the impact of the respective Ru complexes on $A\beta_{40}$ aggregation. In the absence of any Ru complex, densely packed amorphous aggregates were observed for $A\beta_{40}$ (Fig. 5C and S41†). These aggregates were greatly diminished following treatment with the Ru complexes, where diffuse and less dense particles were observed. This allowed for a qualitative assessment for the relative extent of aggregation, where it became evident that **RuBO** consistently had the smallest and most disperse aggregate species. Similar to the DLS results, the densest particulates were observed for **RuO**, while the remaining three complexes had similar, yet subtly different features, which allowed them to be ranked with respect to increasing aggregate density/size as follows: **RuBN** < **RuS** < **RuBS**.

Protein binding

Human serum albumin (HSA) is most abundant protein in blood, and a frequent transporter of various hydrophobic molecules and pharmaceuticals.[51] Within the protein are two well-established binding sites of small molecules, known as Sudlow Site I,[52] which preferentially binds bulky heterocyclic molecules,[53] and Sudlow Site II,[54] which binds aromatic molecules.[53] Previous ruthenium-based therapeutics have an established affinity for HSA, readily forming non-coordinate interactions upon mixing.[55,56] Since this protein does not cross the blood–brain barrier (BBB),[57] binding should be minimized for a potential neurotherapeutic. To assess the association of the prepared Ru complexes with HSA, a competition assay was conducted. For these experiments, HSA was initially treated with dansyl glycine (DG) which selectively binds to Sudlow Site II, yielding a strong fluorescence signal.[58] This mixture was then exposed to gradually increasing amounts of each Ru complex, where any change to DG fluorescence is indicative of its displacement in the binding site *via* the Ru complex. These decreases in fluorescence can be used to construct a Stern–Volmer plot, where conditional binding constants (K') can be obtained.

With increasing amounts of the Ru complexes a concomitant decrease in the DG fluorescence was observed (Fig. S42–46†). These decreases in fluorescence were used to construct a Stern–Volmer plot (Fig. 6) using the equation below; where F_0 is the initial intensity of fluorescence when the competitor (Ru complex, c_{Ru}) concentration is zero, F is the fluorescence intensity when $c_{Ru} > 0$ μM, and the slope of each linear fit affords K' for each Ru complex.[29]

$$\frac{F_0}{F} = 1 + K' c_{Ru}$$

Overall, moderate binding constants were determined for each Ru complex, and are summarized in Table 1, where **RuBO** had the lowest binding affinity and **RuS** had the greatest affinity. These results are somewhat surprising, as they clash with the lipophilicity of the complexes, which has been shown for previous Ru complexes to correlate with HSA binding.[59] However, the K' values obtained are similar to previously reported Ru–arene complexes.[60] Furthermore, the bonding constants obtained for the Ru complexes (3.89–4.48) are well below that of KP1339 (5.32),[29] a well-established Ru(III) anticancer complex that is currently undergoing clinical evaluation (under a new name: BOLD-100).[61]

Modulating Aβ-induced cytotoxicity

While the aggregates of Aβ are one of the established hallmarks of AD, soluble oligomers have been recognized as the active toxic species, representing an important therapeutic target.[62] Therefore, the ability of the prepared Ru complexes to behave as neuroprotective agents was evaluated using an MTT

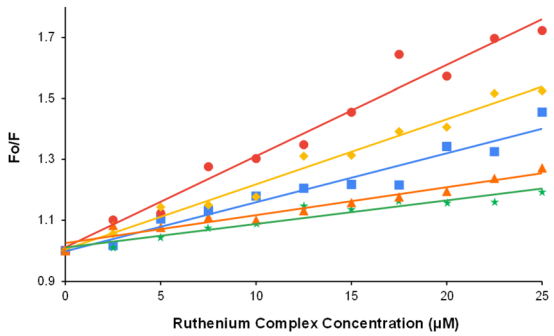

Fig. 6 Stern–Volmer plot of fluorescence competition experiments for complexes **RuO** (■), RuS (●), RuBN (▲), RuBO (★), and RuBS (◆). Binding to HSA was evaluated at Sudlow Site II using DG.

Table 2 Glial cell viability following the addition of equimolar amounts of each respective Ru complex and $A\beta_{42}$ (20 μM) for 24 h as determined by an MTT assay

Treatment	Percent viability
$A\beta_{42}$	76 ± 13
$A\beta_{42}$ + **RuO**	83 ± 6.5
$A\beta_{42}$ + **RuS**	80 ± 10
$A\beta_{42}$ + **RuBN**	84 ± 11
$A\beta_{42}$ + **RuBO**	86 ± 17
$A\beta_{42}$ + **RuBS**	84 ± 10

Table 3 Rankings for the complexes on their respective ability to modulate the aggregation of $A\beta_{40}$, bind to HSA, and diminish the cytotoxicity of $A\beta_{42}$, on a scale of 1–5 (1 = best, 5 = worst)

Complex	ThT	DLS	TEM	HSA	Cytotoxicity	Average
RuO	2	5	5	4	4	4
RuS	3	2	3	2	5	3
RuBN	4	3	2	5	3	3.4
RuBO	1	1	1	1	1	1
RuBS	5	4	4	3	2	3.6

cell viability assay where both the peptide and each Ru complex were co-incubated with *Rattus norvegicus* C6 glioma cells. Following incubation with the peptide alone, a moderate decrease in cell viability was observed (Table 2). For the cells that received treatment with the Ru complexes the average cell viability increased. Although not statistically significant, the trend of increasing cell viability following administration of the complexes is encouraging, as they demonstrate the ability to disrupt the cytotoxic oligomerization of the peptide. A similar trend was observed for previous Ru complexes, where comparable viabilities were seen.[16,17,49]

Conclusion

The impetus behind the current study was the development of Ru(II)–arene complexes with a propensity to modulate the aggregation of soluble Aβ, while also establishing metrics for future development by codifying serum protein affinity. By leveraging previously established SAR where the 2-aminoazoles displayed prominent anti-Aβ activity, five Ru(II)–arene analogs were prepared and studied. The complexes displayed remarkable stability in buffered aqueous media, while also demonstrating the ability to associate with Aβ. Furthermore, by having neutral complexes, the lipophilicity was improved from their Ru(III) predecessors and encroached upon favorable territory for a CNS targeting agent.

To evaluate the ability of the complexes to modulate the aggregation of $A\beta_{40}$, three sequential methods were used: ThT fluorescence, DLS, and TEM imaging. In all cases, following treatment with the individual complexes, disruption of $A\beta_{40}$ aggregation was observed. Furthermore, all five complexes were able to rescue glial cells from $A\beta_{42}$-induced cytotoxicity. Lastly, with HSA recognized as a predominant target for Ru(III) therapeutics *in vivo*,[63,64] the affinity of the prepared complexes for the serum protein was determined. In all cases, the measured binding constants were less than their Ru(III) predecessors,[29] which is encouraging since HSA does not cross the BBB,[57] therefore a strong affinity for the protein would likely curb CNS access.

In terms of performance, the ability of the respective Ru complexes to modulate the aggregation of $A\beta_{40}$, impact the cytotoxicity of $A\beta_{42}$, and coordinate to HSA was tabulated, where for each method of evaluation the complexes were ranked from best to worst (Table 3). This greatly facilitated a ranking of the complexes to determine which complex had the greatest performance overall. **RuBO** separated itself from the pack as the lead candidate, as it consistently outperformed all of the other complexes in every phase of evaluation. Taken together, this demonstrates that 2-aminooxazole ligand was critical to the performance of the **RuBO**. Surprisingly, when comparing the average scores for the remaining four complexes, very similar results were obtained.

Regarding the pharmacological properties of the complexes, **RuBO** persists as a promising lead candidate. While its measured $\log D_{7.4}$ is just outside of the desired range for common CNS targeting agents,[38] the low affinity for HSA is encouraging. Particularly when compared to the Ru(III) anticancer complex KP1339, which despite its affinity for HSA was observed to cross the BBB in BALD mice.[65] Overall, the performance of all five complexes suggests that the Ru–arene scaffold with a 2-aminoheterocyclic ligand is a promising avenue for AD therapeutic development, with **RuBO** leading the way.

Author contributions

MIW designed the study and wrote the initial draft of the manuscript, while all authors contributed to revisions for the final submission. MMW, CCK, and CJM performed the initial synthesis of the complexes used in the study, while DMG, RMH, and KAM repeated the synthesis, completed the characterization, and analysis of the complexes with Aβ and HSA. WWB solved the crystal structures of **RuO**, **RuS**, and **RuBO**, and performed the elemental analysis of all 5 complexes. ES and MAJ performed the cytotoxicity study of the complexes.

Data availability

The data supporting this article have been included as part of the ESI.† Crystallographic data for **RuO**, **RuS**, and **RuBO** have been deposited at the CCDC under 2356322, 2356323 and 2356324, respectively.†

Conflicts of interest

There are no conflicts to declare.

Acknowledgements

The authors are grateful to Bradley M. Kraft and Mary Jo Valenti of St John Fisher University for their assistance with ^{1}H NMR measurements *via* access and use of their Bruker NMR spectrometer. MIW thanks the SUNY Geneseo Chemistry and Biochemistry Department along with the Provost's Office for a generous start-up package.

References

1 A. Alzheimer, R. A. Stelzmann, H. N. Schnitzlein and F. R. Murtagh, *Clin. Anat.*, 1995, **8**, 429–431.
2 *Alzheimer's Dementia*, 2024, **20**, 3708–3821.
3 M. A. DeTure and D. W. Dickson, *Mol. Neurodegener.*, 2019, **14**, 32.
4 A. J. Kuhn and J. Raskatov, *J. Alzheimer's Dis.*, 2020, **74**, 43–53.
5 J. A. Hardy and G. A. Higgins, *Science*, 1992, **256**, 184–185.
6 J. Hardy and D. J. Selkoe, *Science*, 2002, **297**, 353–356.
7 J. Cummings, *Drugs*, 2023, **83**, 569–576.
8 A. Abelein, *Acc. Chem. Res.*, 2023, **56**, 2653–2663.
9 L. M. F. Gomes, J. C. Bataglioli and T. Storr, *Coord. Chem. Rev.*, 2020, **412**, 213255.
10 H. Han, C. G. Cho and P. T. Lansbury, *J. Am. Chem. Soc.*, 1996, **118**, 4506–4507.
11 K. J. Barnham, V. B. Kenche, G. D. Ciccotosto, D. P. Smith, D. J. Tew, X. Liu, K. Perez, G. A. Cranston, T. J. Johanssen, I. Volitakis, A. I. Bush, C. L. Masters, A. R. White, J. P. Smith, R. A. Cherny and R. Cappai, *Proc. Natl. Acad. Sci. U. S. A.*, 2008, **105**, 6813–6818.
12 G. Ma, F. Huang, X. Pu, L. Jia, T. Jiang, L. Li and Y. Liu, *Chem. – Eur. J.*, 2011, **17**, 11657–11666.
13 V. B. Kenche, L. W. Hung, K. Perez, I. Volitakes, G. Ciccotosto, J. Kwok, N. Critch, N. Sherratt, M. Cortes, V. Lal, C. L. Masters, K. Murakami, R. Cappai, P. A. Adlard and K. J. Barnham, *Angew. Chem., Int. Ed.*, 2013, **52**, 3374–3378.
14 M. I. Webb, *Encyclopedia of Inorganic and Bioinorganic Chemistry*, 2023, pp. 1–26, DOI: **10.1002/9781119951438.eibc2846**.
15 S. E. Huffman, G. K. Yawson, S. S. Fisher, P. J. Bothwell, D. C. Platt, M. A. Jones, C. G. Hamaker and M. I. Webb, *Metallomics*, 2020, **12**, 491–503.
16 G. K. Yawson, M. F. Will, S. E. Huffman, E. T. Strandquist, P. J. Bothwell, E. B. Oliver, C. F. Apuzzo, D. C. Platt, C. S. Weitzel, M. A. Jones, G. M. Ferrence, C. G. Hamaker and M. I. Webb, *Inorg. Chem.*, 2022, **61**, 2733–2744.
17 J. T. Ehlbeck, D. M. Grimard, R. M. Hacker, J. A. Garcia, B. J. Wall, P. J. Bothwell, M. A. Jones and M. I. Webb, *J. Inorg. Biochem.*, 2024, **250**, 112424.
18 R. E. Morris, R. E. Aird, P. D. Murdoch, H. M. Chen, J. Cummings, N. D. Hughes, S. Parsons, A. Parkin, G. Boyd, D. I. Jodrell and P. J. Sadler, *J. Med. Chem.*, 2001, **44**, 3616–3621.
19 C. S. Allardyce, P. J. Dyson, D. J. Ellis and S. L. Heath, *Chem. Commun.*, 2001, 1396–1397, DOI: **10.1039/b104021a**.
20 B. S. Murray, M. V. Babak, C. G. Hartinger and P. J. Dyson, *Coord. Chem. Rev.*, 2016, **306**, 86–114.
21 G. Devagi, G. Shanmugam, A. Mohankumar, P. Sundararaj, F. Dallemer, P. Kalaivani and R. Prabhakaran, *J. Organomet. Chem.*, 2017, **838**, 12–23.
22 M. Cuccioloni, V. Cecarini, L. Bonfili, R. Pettinari, A. Tombesi, N. Pagliaricci, L. Petetta, M. Angeletti and A. M. Eleuteri, *Int. J. Mol. Sci.*, 2022, **23**, 8710.
23 C. J. Meiss, P. J. Bothwell and M. I. Webb, *Can. J. Chem.*, 2022, **100**, 18–24.
24 R. Sabate, M. Gallardo and J. Estelrich, *Biopolymers*, 2003, **71**, 190–195.
25 G. M. Sheldrick, *Acta Crystallogr., Sect. A: Found. Adv.*, 2015, **71**, 3–8.
26 G. M. Sheldrick, *Acta Crystallogr., Sect. C: Struct. Chem.*, 2015, **71**, 3–8.
27 N. Chadwick, D. K. Kumar, A. Ivaturi, B. A. Grew, H. M. Upadhyaya, L. J. Yellowlees and N. Robertson, *Eur. J. Inorg. Chem.*, 2015, 4878–4884, DOI: **10.1002/ejic.201500633**.
28 G. K. Yawson, S. E. Huffman, S. S. Fisher, P. J. Bothwell, D. C. Platt, M. A. Jones, G. M. Ferrence, C. G. Hamaker and M. I. Webb, *J. Inorg. Biochem.*, 2021, **214**, 111303.
29 O. Domotor, C. G. Hartinger, A. K. Bytzek, T. Kiss, B. K. Keppler and E. A. Enyedy, *J. Biol. Inorg. Chem.*, 2013, **18**, 9–17.
30 J. G. Malecki, *Struct. Chem.*, 2012, **23**, 461–472.
31 E. J. Anthony, E. M. Bolitho, H. E. Bridgewater, O. W. L. Carter, J. M. Donnelly, C. Imberti, E. C. Lant, F. Lermyte, R. J. Needham, M. Palau, P. J. Sadler, H. Y. Shi, F. X. Wang, W. Y. Zhang and Z. J. Zhang, *Chem. Sci.*, 2020, **11**, 12888–12917.
32 K. Ghebreyessus, A. Peralta, M. Katdare, K. Prabhakaran and S. Paranawithana, *Inorg. Chim. Acta*, 2015, **434**, 239–251.
33 M. Muralisankar, J. R. Chen, J. Haribabu and S. C. Ke, *Int. J. Mol. Sci.*, 2023, **24**, 11896.
34 K. J. Kilpin, S. M. Cammack, C. M. Clavel and P. J. Dyson, *Dalton Trans.*, 2013, **42**, 2008–2014.
35 F. Wang, H. M. Chen, S. Parsons, I. D. H. Oswald, J. E. Davidson and P. J. Sadler, *Chem. – Eur. J.*, 2003, **9**, 5810–5820.
36 A. M. Seddon, D. Casey, R. V. Law, A. Gee, R. H. Templer and O. Ces, *Chem. Soc. Rev.*, 2009, **38**, 2509–2519.
37 OECD, *Test #107: Partition Coefficient (n-octanol/water): Shake Flask Method*, OECD Publishing, 1995.
38 H. van de Waterbeemd, G. Camenisch, G. Folkers, J. R. Chretien and O. A. Raevsky, *J. Drug Targeting*, 1998, **6**, 151–165.
39 H. Pajouhesh and G. R. Lenz, *NeuroRx*, 2005, **2**, 541–553.
40 A. Daina, O. Michielin and V. Zoete, *Sci. Rep.*, 2017, **7**, 42717.
41 V. A. Streltsov, V. C. Epa, S. A. James, Q. I. Churches, J. M. Caine, V. B. Kenche and K. J. Barnham, *Chem. Commun.*, 2013, **49**, 11364–11366.

42 X. H. Wang, X. Y. Wang, C. L. Zhang, Y. Jiao and Z. J. Guo, *Chem. Sci.*, 2012, **3**, 1304–1312.
43 S. A. Kozin, S. Zirah, S. Rebuffat, G. H. B. Hoa and P. Debey, *Biochem. Biophys. Res. Commun.*, 2001, **285**, 959–964.
44 K. G. Malmos, L. M. Blancas-Mejia, B. Weber, J. Buchner, M. Ramirez-Alvarado, H. Naiki and D. Otzen, *Amyloid*, 2017, **24**, 1–16.
45 P. K. Singh, M. Kumbhakar, H. Pal and S. Nath, *J. Phys. Chem. B*, 2010, **114**, 2541–2546.
46 C. Xue, T. Y. W. Lin, D. Chang and Z. F. Guo, *R. Soc. Open Sci.*, 2017, **4**, 160696.
47 R. Tycko, *Protein Sci.*, 2014, **23**, 1528–1539.
48 A. M. Streets, Y. Sourigues, R. R. Kopito, R. Melki and S. R. Quake, *PLoS One*, 2013, **8**, e54541.
49 B. J. Wall, M. F. Will, G. K. Yawson, P. J. Bothwell, D. C. Platt, C. F. Apuzzo, M. A. Jones, G. M. Ferrence and M. I. Webb, *J. Med. Chem.*, 2021, **64**, 10124–10138.
50 J. Stetefeld, S. A. McKenna and T. R. Patel, *Biophys. Rev.*, 2016, **8**, 409–427.
51 D. Sleep, *Expert Opin. Drug Delivery*, 2015, **12**, 793–812.
52 G. Sudlow, D. J. Birkett and D. N. Wade, *Mol. Pharmacol.*, 1975, **11**, 824–832.
53 U. Kragh-Hansen, V. T. G. Chuang and M. Otagiri, *Biol. Pharm. Bull.*, 2002, **25**, 695–704.
54 G. Sudlow, D. J. Birkett and D. N. Wade, *Mol. Pharmacol.*, 1976, **12**, 1052–1061.
55 N. Cetinbas, M. I. Webb, J. A. Dubland and C. J. Walsby, *J. Biol. Inorg. Chem.*, 2010, **15**, 131–145.
56 M. I. Webb and C. J. Walsby, *Dalton Trans.*, 2011, **40**, 1322–1331.
57 F. Kratz, *J. Controlled Release*, 2008, **132**, 171–183.
58 N. Muller, F. Lapicque, E. Drelon and P. Netter, *J. Pharm. Pharmacol.*, 1994, **46**, 300–304.
59 S. W. Chang, A. R. Lewis, K. E. Prosser, J. R. Thompson, M. Gladkikh, M. B. Bally, J. J. Warren and C. J. Walsby, *Inorg. Chem.*, 2016, **55**, 4850–4863.
60 S. Hairat and M. Zaki, *J. Organomet. Chem.*, 2021, **937**, 121732.
61 B. Happl, T. Balber, P. Heffeter, C. Denk, J. M. Welch, U. Koester, C. Alliot, A. C. Bonraisin, M. Brandt, F. Haddad, J. H. Sterba, W. Kandioller, M. Mitterhauser, M. Hacker, B. K. Keppler and T. L. Mindt, *Dalton Trans.*, 2024, **53**, 6031–6040.
62 M. Tolar, J. Hey, A. Power and S. Abushakra, *Int. J. Mol. Sci.*, 2021, **22**, 6355.
63 J. M. Rademaker-Lakhai, D. van den Bongard, D. Pluim, J. H. Beijnen and J. H. M. Schellens, *Clin. Cancer Res.*, 2004, **10**, 3717–3727.
64 C. G. Hartinger, M. A. Jakupec, S. Zorbas-Seifried, M. Groessl, A. Egger, W. Berger, H. Zorbas, P. J. Dyson and B. K. Keppler, *Chem. Biodivers.*, 2008, **5**, 2140–2155.
65 A. K. Bytzek, G. Koellensperger, B. K. Keppler and C. G. Hartinger, *J. Inorg. Biochem.*, 2016, **160**, 250–255.